# Evaporation Structures of Solvent Drops Evaporating from Polymer Surfaces: Influence of Molar Mass

*Dedicated to the 65th birthday of Hans W. Spiess*

Guangfen Li, Karlheinz Graf, Elmar Bonaccurso, Dmytro S. Golovko, Andreas Best, Hans-Jürgen Butt*

When a solvent drop evaporates from a polymer surface, a characteristic structure remains. To analyze the structure formation during evaporation we deposited microdrops of ethyl acetate on planar PEMA and toluene on PS. The shape of the evaporation structures depends on the molar mass of the polymer, the number of droplets deposited, and the specific polymer/solvent combination. Crater-like structures with a flat bottom were observed for PEMA. With PS, dot-like protrusions were observed for low and intermediate molar masses; for $\overline{M}_w \geq 210$ kDa, crater-like rims with a depression in the center were formed. These structures are interpreted based on four different processes occurring during evaporation.

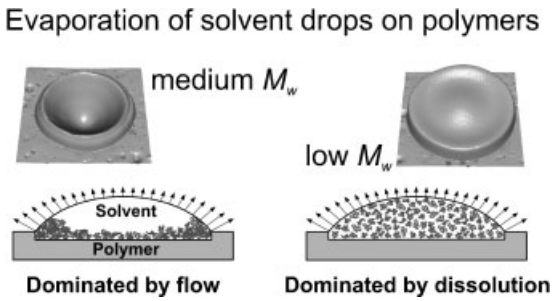


## Introduction

The evaporation of drops of pure liquids from planar, inert solid surfaces has been studied in detail and is well understood.[1–13] Far less understood is the evaporation of liquids from soluble surfaces. In particular the evaporation of solvent drops from polymer surfaces is a complex process, because the polymer is dissolved in the solvent, and at the same time solvent molecules diffuse into the polymer.[14,15] In addition, the viscosity of the mixture and the diffusion constant of the liquid molecules depend on the local concentration. Interest in a better understanding of the evaporation of solvent drops from polymers recently increased because they are used to develop microstructures on polymer surfaces for a variety of applications.[16–19]

The aim of this paper is to better understand the structure formation during the evaporation of solvent drops from soluble surfaces. In addition, the usefulness of topographic structures left by a drying solvent drop on a polymer surface to measure the molar mass is analyzed. As examples we studied toluene drops drying on polystyrene (PS) surfaces and ethyl acetate evaporating from poly(ethyl methacrylate) (PEMA). The liquid drops used in this study were produced by an ink-jet microdropper. Using an ink-jet allows small drops to be deposited. It also allows more

G. Li, K. Graf, E. Bonaccurso, D. S. Golovko, A. Best, H.-J. Butt
Max Planck Institute for Polymer Research, Ackermannweg 10, D-55128 Mainz, Germany
E-mail: butt@mpip-mainz.mpg.de
K. Graf
Center of Micro- and Nanochemistry and Engineering (Cμ), University of Siegen, Germany


*Macromol. Chem. Phys.* **2007**, *208*, 2134–2144
© 2007 WILEY-VCH Verlag GmbH & Co. KGaA, Weinheim
DOI: 10.1002/macp.200700122

drops to be deposited at the same position while or after the previous drop has evaporated. This adds another dimension to the possibilities of creating surface topologies and using them to analyze the molar mass of the underlying substrate. The surface structures left on the polymer surface were less than 200 μm in diameter and 3 μm in height/depth. Therefore the technique is almost non-invasive and little material is required. It is a relative method and depends on the specific chemical structure of the polymer and the nature of the solvent.

## Experimental Part

Polystyrene (PS) was synthesized by anionic polymerization. The molar masses and polydispersities were $\overline{M}_w = 20.9$, 24.3, 29.6, 62.5, 97.5, 210, 339, 643, 1 102, 1 445 kDa and $\overline{M}_w/\overline{M}_n = 1.03$, 1.05, 1.03, 1.06, 1.04, 1.07, 1.07, 1.10, 1.09, 1.16, respectively. To produce flat, smooth surfaces, PS powder was compression-molded at 160 °C under vacuum into transparent disks that were 25 mm wide (except for PS of $\overline{M}_w = 20.9$ kDa, which formed an opaque sample). The PS samples were cleaned with methanol (HPLC grade) in an ultrasonic bath for 15 min prior to the deposition of toluene drops (HPLC grade, Merck KGaA, Darmstadt, Germany, surface tension at 20 °C: $\gamma = 28.4\ \mathrm{mN \cdot m^{-1}}$).

Poly(ethyl methacrylate) (PEMA, PSS GmbH, Mainz, Germany) with molar masses of $\overline{M}_w = 4.7$, 7.5, 45, 142, 500 kDa and polydispersity indices of $\overline{M}_w/\overline{M}_n = 1.08$, 1.07, 1.05, 1.02, 1.11, respectively, was compression-molded as a powder at 100 °C under vacuum into transparent disks that were 25 mm wide. The PEMA samples were rinsed with pure water several times before depositing ethyl acetate drops ($CH_3CH_2OCOCH_3$, analytical grade, Sigma-Aldrich, Chemie GmbH, Germany; $\gamma = 23.8\ \mathrm{mN \cdot m^{-1}}$ at 20 °C).

Solvent drops were placed onto the polymer surfaces with a home-made piezoelectric droplet generator (Verfahrenstechnik, Universität Bremen, Germany). Each droplet was expelled by contraction impulses of the piezo of 1 μs, located around an adapted drop-on-demand nozzle at a distance of approximately 0.3 mm from the sample. The frequency of the drop expulsion can be in the range of about 1 kHz to some seconds. The nozzle had outer and inner diameters of 1 mm and 45 μm, respectively. The drops had diameters of 40–60 μm and thus a typical volume of $V \approx 50$ pL was ejected. A camera system consisting of an objective 5× (Mitutoyo, Japan), a 6.5× ultra-zoom tube (Navitar Inc. Rochester, NY, USA) and a uEye UI-2210-C, 1/2″ CCD camera (VGA IDS Imaging Development Systems GmbH, Obersulm, Germany), together with a white-light source (KL 1500 LCD, Schott, Mainz, Germany) were used to visualize the process. The optical resolution was about 1 μm. Digitized images were stored and analyzed (1.05 μm pixel size). The height and diameter of the droplets in the images were measured manually. From the derived drop height $h_0$ and contact radius $a$, the contact angle $\Theta$ was calculated as $\Theta = 2\ \arctan(h_0/a)$.

After drop evaporation the topography of the polymer surface was imaged with a three-dimensional optical measurement system based on white-light confocal microscopy of the disk-scanning type (μsurf, NanoFocus AG, Oberhausen, Germany). Using a 20× or 50× objective, the resolution was 1.5 and 0.6 μm laterally and 5 and 2 nm in height, respectively.

To characterize the optical properties of the evaporation structures, we used a commercial laser scanning confocal microscope (Carl Zeiss, Göttingen, Germany) consisting of the LSM 510 module and the inverted microscope model Axiovert 200M. A Plan-Neofluar 10× objective with a numerical aperture of 0.3 and a working distance of 5.6 mm was used. The optical system was modified by adding an external 5 mW helium-neon laser working at 633 nm, aligned perpendicular to the *xy* scanning plane of the microscope and collinear to the objective lens. In order to generate a plane wavefront the laser beam was expanded 10 times using a beam expander, working in Keplerian mode. This modification enabled illumination of the samples in the transmitted-light configuration. For the reflected-light configuration, the 543 nm line of a 1 mW helium-neon laser was used. The transmitted and reflected light collected from the objective was separated with a dichroic mirror and routed to two independent channels. In one channel, a band-pass filter transmitting in the range from 500–550 nm was chosen to detect the light at 543 nm. In the second channel a long-pass filter with a cut-on wavelength of 560 nm was applied. For detection, photomultipliers were used. By using pinholes with a diameter of 71 μm for the green light and 78 μm for the red light in the confocal position, in front of the corresponding detector, light from thin optical slices with a thickness of about 12 μm could be collected from the focal plane.

## Results and Discussion

### Observation of the Evaporation Process

When depositing solvent drops onto the polymer surfaces by a nozzle, the optically visible evaporation process typically took 0.3 s. During evaporation, the contact radius was constant and the contact angle decreased (Figure 1). The contact angle of toluene on PS was lower than that of ethyl acetate on PEMA. Correspondingly, the contact radius was larger for toluene/PS. For example, for PS of $\overline{M}_w = 210$ kDa, the initial contact angle was $\Theta = 13 \pm 1°$ and the contact radius was $a = 81 \pm 5$ μm, leading to an initial volume of $\approx 10^5\ \mu m^3$. For ethyl acetate on PEMA of $\overline{M}_w = 142$ kDa, the respective values were $\Theta = 22 \pm 1°$, $a = 57 \pm 3$ μm, and initial volume $\approx 6 \times 10^4\ \mu m^3$. These values were characteristic also for the other molecular weights. The errors are typical differences measured between different experiments with polymers of similar molar mass. Since the initial volumes of the toluene drops on PS were bigger than those of ethyl acetate on PEMA, the apparent evaporation time of toluene from PS of toluene from PS (0.33 s) was longer than that for ethyl acetate from PEMA (0.27 s). The "apparent" evaporation time was derived by extrapolating the decreasing volume-versus-time to zero volume. It does not correspond to the time required to evaporate all of the solvent: some solvent will diffuse into the polymer and remain in the polymer for


© 2007 WILEY-VCH Verlag GmbH & Co. KGaA, Weinheim

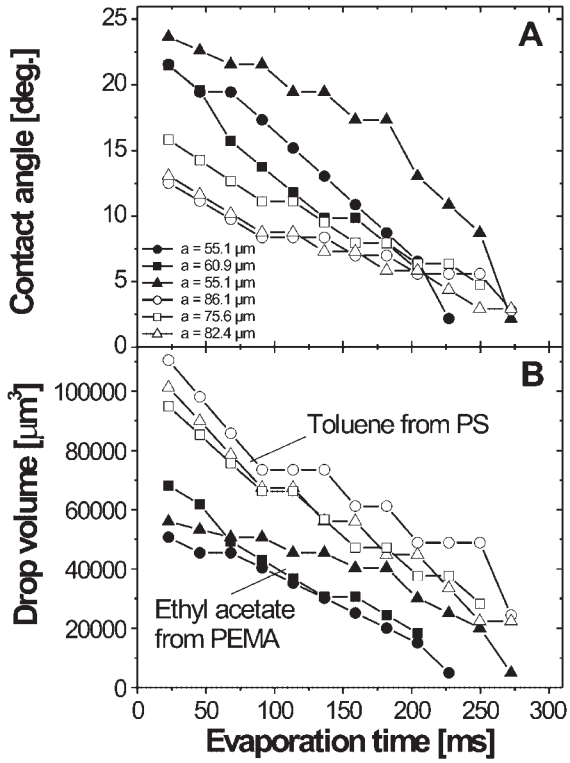


*Figure 1.* (A) Contact angle and (B) drop volume versus time for three typical drops of ethyl acetate evaporating from PEMA ($\overline{M}_w = 142$ kDa, filled symbols) and three drops of toluene evaporating from PS ($\overline{M}_w = 210$ kDa, open symbols). The contact radii in the six cases were 55.1, 60.9, 55.1 μm for ethyl acetate on PEMA, and 86.1, 75.6, 82.4 μm for toluene on PS, respectively.

much longer times. This effect explains the strongly reduced vapor pressure.

From the evaporation rate, the diffusion constant of the solvent molecules in the vapor phase can be calculated. The evaporation rate, that is the decrease in solvent volume per unit time, $|dV/dt|$, can be derived assuming that the diffusion of molecules in the gas phase is rate limiting, that a steady state is reached at each stage of evaporation, that the temperature is constant, and that the vapor pressure of the liquid far away from the drop is zero:[3]

$$\left|\frac{dV}{dt}\right| = 2\pi D_t R_c f \frac{P_0 M}{\rho RT} \quad (1)$$

Here, $D_t$ is the diffusion constant of solvent in air, $R_c$ is the radius of curvature of the drop, $P_0$ is the vapor pressure of the solvent, $M$ is its molar mass, $R$ is the gas constant, $T$ the temperature, and $\rho$ is the liquid density. The function $f$ is given by $f = (0.00008957 + 0.6333\Theta + 0.116\Theta^2 - 0.08878\Theta^3 + 0.01033\Theta^4)$. For toluene evaporating from PS we have an evaporation rate of $4.2 \times 10^5$ $\mu m^3 \cdot s^{-1}$ at a contact angle of $\Theta = 13.3°$ at the beginning. With $f = 0.1522$, $R_c = 334$ μm, $P_0 = 3.79$ kPa, $M = 92.13$ g·mol$^{-1}$, $\rho = 866$ kg·m$^{-3}$ and at 25 °C, we find a diffusion coefficient $D_t = 8.2 \times 10^{-6}$ m$^2$·s$^{-1}$. This agrees well with a value of $8.0 \times 10^{-6}$ m$^2$·s$^{-1}$ measured previously in tube and sessile drop evaporation experiments[20] and $8.0 \times 10^{-6}$ m$^2$·s$^{-1}$ measured from a toluene drop evaporating from an inert surface.

After 0.20 s the corresponding values are $2.6 \times 10^5$ $\mu m^3 \cdot s^{-1}$ at a contact angle of $\Theta = 5.9°$, $f = 0.0664$, and $R_c = 780$ μm. Assuming that the diffusion coefficient of toluene does not change, we can calculate the vapor pressure of toluene after 0.2 s to be 3.08 kPa. We attribute this reduction in vapor pressure to the presence of dissolved PS, according to Raoult's law. Dissolved PS should reduce the vapor pressure of toluene.

For ethyl acetate evaporating from PEMA we have an evaporation rate of $2.4 \times 10^5$ $\mu m^3 \cdot s^{-1}$ at a contact angle of $\Theta = 22.2°$ at the beginning. With $f = 0.2577$, $R_c = 151$ μm, $P_0 = 12.6$ kPa, $M = 88.12$ g·mol$^{-1}$, $\rho = 894.5$ kg·m$^{-3}$ and at 25 °C, we find a diffusion coefficient $D_t = 1.9 \times 10^{-6}$ m$^2$·s$^{-1}$ for ethyl acetate in air at normal pressure. After 0.20 s the corresponding values are $2.4 \times 10^5$ $\mu m^3 \cdot s^{-1}$ at a contact angle of $\Theta = 8.4°$, $f = 0.0951$, and $R_c = 440$ μm. Assuming that the diffusion coefficient of ethyl acetate does not change we can calculate the vapor pressure of ethyl acetate after 0.2 s to be 4.4 kPa. Since ethyl acetate evaporated faster than toluene, after 0.2 s the volume ratio of ethyl acetate in the polymer containing droplet is even lower than that of toluene evaporating from PS. This effect explains the strongly reduced vapor pressure. Summarizing, the diffusion coefficient for ethyl acetate in air dominates the slow evaporation rate and counteracts the higher vapor pressure compared to toluene on PS. An additional effect comes from the lower wettability of ethyl acetate on PEMA. A drop of the same volume covers a lower contact area on the polymer than toluene on PS, leading to a lower radius of curvature and a higher contact angle, i.e. a higher value of f. For ethyl acetate on PEMA the product of both is smaller than for toluene of PS, contributing to the lower evaporation rate in addition to the diffusion coefficient (cf. Equation (1)).

### Crater-Like Structures

When comparing the evaporation structures left by different combinations of solvent and polymer (Figure 2, 3) some characteristic features are generally observed, while others are qualitatively and quantitatively different and depend on the specific combination. One characteristic feature generally observed are crater-like rings with a depression in the middle. Such crater-like structures have been described before.[14,16,21] In PS the central part is typically shaped like an inverted, spherical cap, while for PEMA the central depression is flat. The formation of


© 2007 WILEY-VCH Verlag GmbH & Co. KGaA, Weinheim
DOI: 10.1002/macp.200700122

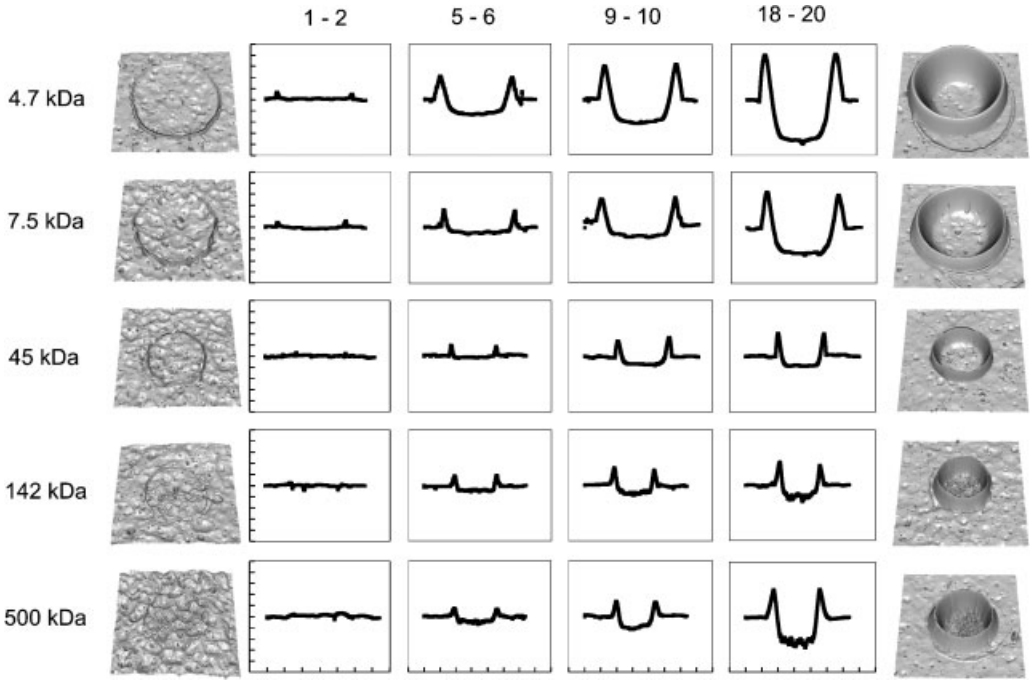


*Figure 2.* Surface plots (left and right) and cross-sections (middle) of structures left by ethyl acetate drops deposited by the ink-jet on poly(ethyl methacrylate) with different molar masses, 1–2 h after drying. The height in the surface plots is automatically rescaled so that height is only in relative units. For the cross-sections, the ticks are spaced 1 μm vertically and 50 μm horizontally. The four height profiles for each molar mass refer to depositions of 1–2, 5–6, 9–10, and 18–20 drops deposited at intervals of 0.5 s on the same spot.

crater-like structures can be understood, based on a model developed to interpret the formation of ring-shaped "coffee stains".[14,16,18,22–26] When the solvent gets into contact with the substrate, polymer chains are dissolved. In a pinned evaporating drop, a radial flow occurs to compensate the difference in volume change and evaporation rate across the drop.[27] In the edge region of the drop, the evaporation rate is high because the available angle of evaporation is increased (for $\Theta < 90^\circ$), but the change in volume is restricted by the pinned contact line. In the center, on the other hand, the evaporation rate is lower but the volume changes drastically. The radial flow supplies the liquid from the center to the edge region to compensate the difference. The dissolved polymer is carried with the flow and finally deposited at the rim.

## Multiple Drops

When depositing multiple drops at the same place and allowing 0.5 s for each drop to evaporate before the next drop was deposited, the evaporation structures became more pronounced. For ethyl acetate on PEMA the protruding rim became higher and the central depression deeper. This indicates that the same liquid flow to the rim and evaporation pattern prevails for each drop.

For toluene on PS with a molecular weight below 100 kDa the picture changed qualitatively. For only a few drops a central depression was formed, while for 10 and more drops a dot-like elevation formed in the center. Two interpretations are possible: firstly, the crater-like structure formed by the first few drops influences the flow and evaporation pattern for the subsequent drops; secondly, toluene diffuses into PS; some toluene of the first drop is certainly left when the second drop arrives. The presence of toluene will cause the polymer-polymer interactions to be gradually replaced with polymer-solvent interactions. Thus when the second drop wets the PS surface the polymer chains are already solvated. This accelerates the total dissolution process and more PS gets dissolved before the majority of the solvent has evaporated.

## Influence of Molar Mass for PEMA

With PEMA for all molar masses and irrespective of the number of drops deposited, crater-like structures are formed. The depth of the craters (as counted from the mean height of the rim) decreased with increasing molar mass (Figure 4A). The reason for the decrease in depth is probably the reduced dissolution rate of polymer with a high molar mass. If less material gets dissolved, less material is transported to the rim.

The fact that the evaporation structure depends on the molar mass of the polymer may be able to be used to determine the molar mass. One simple parameter, which, after calibration, can be used to determine the molar mass, is the depth of the crater-like structure. Using 15 to 20


© 2007 WILEY-VCH Verlag GmbH & Co. KGaA, Weinheim

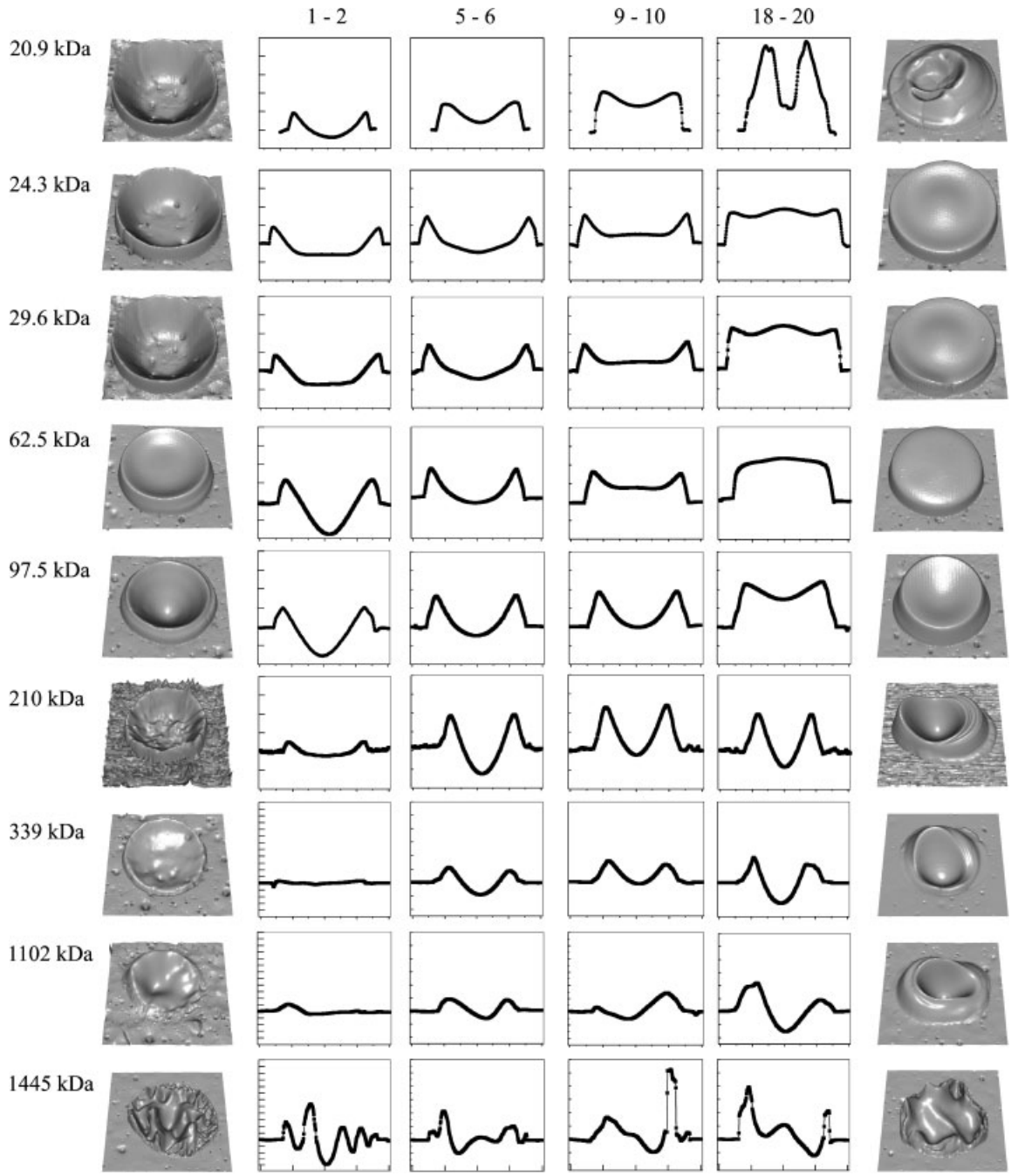


*Figure 3.* Surface plots (left and right) and cross-sections (middle) of structures left by toluene drops deposited by the inkjet on polystyrene with different molar masses, 1–2 h after drying. The height in the surface plots is automatically rescaled so that height is only in relative units. For the cross-sections the ticks are spaced 1 μm vertically and 50 μm horizontally. The four height profiles for each molar mass refer to depositions of 1–2, 5–6, 9–10, and 18–20 drops deposited at intervals of 0.5 s on the same spot.

drops leads to the best sensitivity. Unfortunately, if the molar mass is above $\overline{M}_w = 45$ kDa, the depth increases again, thus providing a non-monotonic function of $\overline{M}_w$. To discriminate the higher molar masses another characteristic feature, which is observed for PEMA and PS, can be utilized: the evaporation structure becomes asymmetric and irregular. In cross-sections on evaporation structures in PEMA this appeared as a "noisy" line at the bottom of the craters for $\overline{M}_w = 142$ kDa and 500 kDa. For lower molar masses the bottom of crater appeared smooth.

For ethyl acetate on PEMA the craters at low molar mass were wider than the craters at intermediate and high molar mass: the higher the molar mass, the smaller the crater width (Figure 4B). Usually the second drop spreads


*Macromol. Chem. Phys.* **2007**, *208*, 2134–2144
© 2007 WILEY-VCH Verlag GmbH & Co. KGaA, Weinheim
DOI: 10.1002/macp.200700122

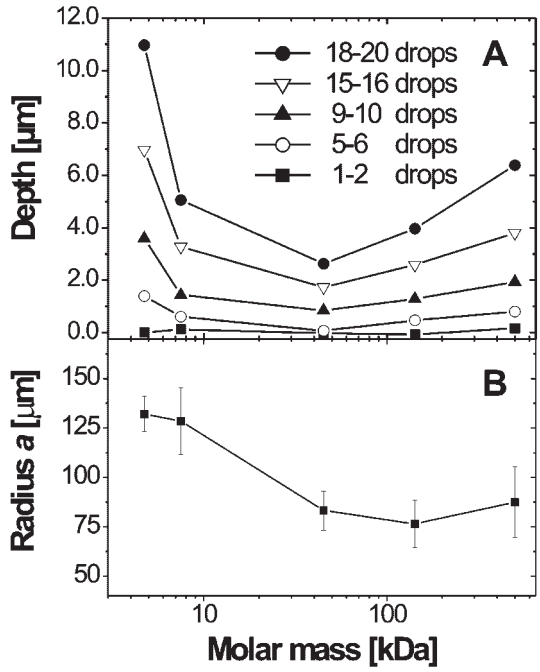


*Figure 4.* (A) Depth and (B) contact radius of craters left on PEMA after evaporation of different numbers of drops of ethyl acetate. The depth is the height difference between the depression in the center of the crater and the mean height of the rim. For the contact radius, only results for the first drops are shown. Subsequent drops spread to the same radius.

to the same radius as the first one. For this reason only the results for the first drop are shown in Figure 4B. In only a few cases, the second drop with the same solvent volume tended to shrink and create another rim inside the first rim. After that, the rest of drops were directed into this second rim.

### Evaporation Structures on PS

After evaporation of toluene from low and intermediate molar mass PS, the volume of the polymer had obviously increased (Figure 3). This effect increased with increasing number of drops. The bottom of the evaporation craters for $\overline{M}_w \leq 97.5$ kDa was above the level of the original polymer surface. At $\overline{M}_w = 62.5$ kDa even a dot-like structure was observed when depositing 18–20 on one spot. A similar effect was observed when carefully looking at PEMA after the first drop had evaporated: for high molar mass the polymer swelled. We interpret this swelling of polymer due to a permanent local decrease of the density (increase in free volume) with solvent molecules staying in.

At high molar masses of PS the craters became asymmetric. With increasing $\overline{M}_w$, the degree of asymmetry and the length scale, on which the asymmetric feature appeared, decreased. At $\overline{M}_w = 339$ kDa, the outer ridge typically showed a height modulation; it was significantly higher on one side than on the opposite one. The length scale of the asymmetry was of the order of 200–300 μm. At $\overline{M}_w = 1\,445$ kDa, the crater was filled with an irregular pattern of small depressions and protrusions with a width of typically 50 μm.

A closer look at the surface topologies reveals different classes of symmetry. For low and intermediate molar masses between 24.3 and 210 kDa the resulting topology showed nearly axial symmetry. Nevertheless, the topology changed from centrally bulged (24.3 kDa) to over-dimpled (29.6 kDa) to concave (210 kDa). This observation is described in the literature for an evaporating sessile droplet with dissolved polymer on an insoluble substrate when the polymer concentration is decreased.[28] It was discussed as a bulging in the center of the droplet for an initially-high polymer concentration[29] and a coffee-stain-like effect for lower initial concentrations. In our case the polymer concentration is mediated through the molar mass. Thus, it confirms our interpretation and additionally suggests that the basic principles for insoluble substrates can be transferred to the description of the process on soluble ones. Consequently, for much higher molar masses above 210 kDa the polymer concentration should be increasingly lower. Since it is associated with an increasing asymmetry of the resulting surface topology, instabilities as an origin for theses structures are likely. For a decreasing polymer concentration with increasing molar mass of the substrate, the viscosity inside the droplet decreases. This leads to an increasing Marangoni number und thus might favor a Marangoni-type convection inside the droplet.[10,30,31] Undulations with characteristic distances in the order of 50 μm were found for the dissolution of PMMA layers into solvent droplets.[32]

### Modes of Evaporation

Evaporation structures left by an evaporating solvent are determined by at least three processes: (1) the dissolution of polymer; (2) the radial flow of the solvent caused by evaporation; and (3) the diffusion of dissolved polymer in the solvent. To analyze structure formation it is instructive to consider two extreme cases (Figure 5); for simplicity we assume the dissolution rate to be independent on the concentration of already-dissolved polymer:

- Fast flow: if we assume that the evaporation-driven flow is much faster than the equilibration due to diffusion, the dissolved material is deposited mainly at the periphery of the drop and a rim is formed.
- Fast diffusion: if we assume that the diffusion of the dissolved molecules is much faster than the evaporation-driven flow, we have an equal concentration of dissolved molecules in the whole solvent at all times. The final pattern of the deposited material is then


© 2007 WILEY-VCH Verlag GmbH & Co. KGaA, Weinheim

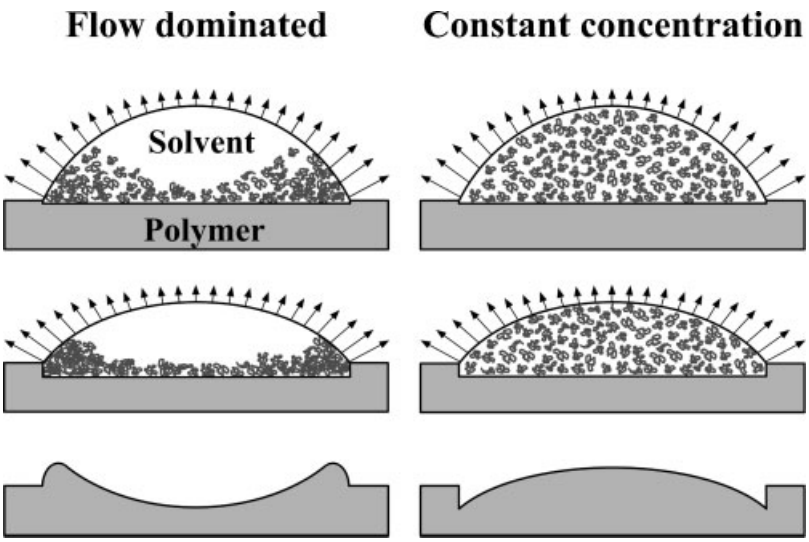


*Figure 5.* Schematic depiction of two extreme cases of solvent evaporation.

similar to the shape of the drop. Polymer is mainly deposited in the center and forms a dot-like structure.

A real evaporation structure is between the two extreme cases and the final structure will depend on the time and length scales over which the three processes occur. We now estimate the time and length scales of the three processes.

### Dissolution

To estimate the rate of dissolution one can measure the depth of craters formed, after the first drop has been deposited. Assuming that most of the dissolved materials is transported to the rim by the evaporation-driven flow, the depth of the crater should be a measure of the amount dissolved. When plotting the depth versus the molar mass (Figure 6) it is obvious, that the dissolution of PS in toluene is more efficient than the dissolution of PEMA in ethyl acetate. The maximal depth in the center is 1.8 μm for PS ($\overline{M}_w = 62$ kDa) and only 0.12 μm for PEMA ($\overline{M}_w = 7.5$ kDa). Thus the lower limit for the dissolution rate is 1.8 μm per 0.33 s = 5.5 $\mu m \cdot s^{-1}$ and 0.12 μm per 0.27 s = 0.44 $\mu m \cdot s^{-1}$, respectively.

The plot of depth versus molar mass shows a maximum in depth (minimum in height) for both solvent/polymer combinations. For PEMA this is at a lower molar mass than for PS. This corresponds to the lower entanglement molar mass of PEMA of $\overline{M}_e = 8.6$ kDa as compared to that of PS of $\overline{M}_e = 18.1$ to 19.1 kDa.[33–35] One would expect the dissolution rate to increase with decreasing molar mass because entanglement, which resists dissolution, is lower. This, however, does not correspond to the depth of craters. In addition, for low molar mass PEMA (4.7 kDa) no change in depth at all was observed. Thus as a second process swelling must be present. Swelling of the polymer is stable even when keeping the polymer in air and giving the solvent several hours to evaporate.

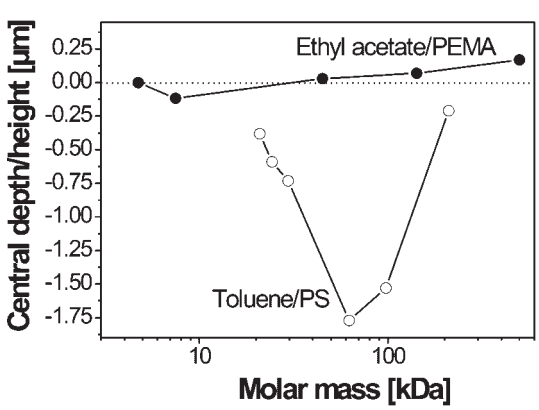


*Figure 6.* Central depth/height of the evaporation structures versus molar mass of the polymer substrate after evaporation of one drop of ethyl acetate on PEMA and toluene on PS, respectively.

### Evaporation-Driven Flow

When the drop evaporates with a pinned contact line, a radial flow occurs to compensate the difference in volume change and evaporation rate across the drop (Figure 7). We estimated the velocity of the flow $v$ in our system from

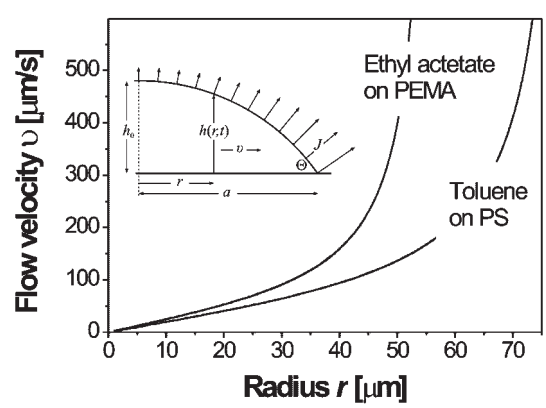


*Figure 7.* Radial flow velocity in an evaporating drop, calculated for the initial stage with Equation (7). The parameters used were estimated from experiments with ethyl acetate drops evaporating from PEMA ($h_o = 11.0$ μm, $\lambda = 0.430$, $dh_o/dt = -41$ $\mu m \cdot s^{-1}$, $dV/dt = -2.2 \times 10^5$ $\mu m^3 \cdot s^{-1}$) and toluene drops evaporating from PS ($h_o = 9.5$ μm, $\lambda = 0.461$, $dh_o/dt = -29$ $\mu m \cdot s^{-1}$, $dV/dt = -3.0 \times 10^5$ $\mu m^3 \cdot s^{-1}$). At the top left, a schematic of an evaporating drop illustrates the parameters.


*Macromol. Chem. Phys.* **2007**, *208*, 2134–2144
© 2007 WILEY-VCH Verlag GmbH & Co. KGaA, Weinheim
DOI: 10.1002/macp.200700122

the equation of continuity assuming laminar flow:[24]

$$v = -\frac{1}{\rho r h}\int_0^r r'\left(\rho\frac{dh}{dt} + J(r',t)\sqrt{1+\left(\frac{dh}{dr'}\right)^2}\right)dr' \quad (2)$$

Here, $v$ is the mean flow velocity in radial direction at a given radial coordinate $r$; $h$ is the height of a drop at radius $r$ and $J$ is the evaporation flux from the surface of the drop in $kg \cdot m^{-2} \cdot s^{-1}$. The height was calculated with the assumption of a hemispherical drop:

$$h(r,t) = \sqrt{\left(\frac{h_0^2 + a^2}{2h_0}\right)^2 - r^2} - \frac{a^2 - h_0^2}{2h_0} \quad (3)$$

Here, $h_0$ is the height in the center. The evaporation flux was calculated according to:[24]

$$J \approx J_0\left[1-(r/a)^2\right]^{-\lambda} \text{ with } \lambda = (90^\circ - \Theta)/(180^\circ - \Theta) \quad (4)$$

For small contact angles and under constant contact-radius conditions we can integrate Equation (2):[36]

$$v = \frac{1}{2rh}\cdot\frac{J_0}{(1-\lambda)\rho}\cdot\left\{\frac{a^2 - r^2}{\left[1-(r/a)^2\right]^{\lambda}} - a^2\right\} - \frac{1}{2rh}\cdot\frac{1}{h_0^2}\frac{dh_0}{dt}\cdot\left\{\frac{r^2}{2}\left(h_0^2 - a^2\right) - \frac{1}{12h_0^2}\left[\left(h_0^2+a^2\right)^2 - 4r^2h_0^2\right]^{3/2} + \frac{\left(h_0^2+a^2\right)^3}{12h_0^2}\right\} \quad (5)$$

To determine the flux $J_0$ in Equation (4) we integrate the total flux to obtain the decrease in volume:

$$-\rho\frac{dV}{dt} = 2\pi\int_0^a rJ\,dr = \frac{\pi a^2 J_0}{(1-\lambda)} \quad (6)$$

Please note that the volume decreases and $dV/dt < 0$. Inserting this into Equation (5) leads to

$$v = -\frac{1}{2rh}\cdot\frac{1}{\pi a^2}\frac{dV}{dt}\cdot\left\{\frac{a^2 - r^2}{\left[1-(r/a)^2\right]^{\lambda}} - a^2\right\} - \frac{1}{2rh}\cdot\frac{1}{h_0^2}\frac{dh_0}{dt}\cdot\left\{\frac{r^2}{2}\left(h_0^2 - a^2\right) - \frac{1}{12h_0^2}\left[\left(h_0^2+a^2\right)^2 - 4r^2h_0^2\right]^{3/2} + \frac{\left(h_0^2+a^2\right)^3}{12h_0^2}\right\} \quad (7)$$

The flow velocities were calculated for two typical cases. For ethyl acetate evaporating from PEMA we used an initial central height of $h_0 = 11.0$ μm, a typical contact radius of $a = 57$ μm, an initial volume of $V = 6 \times 10^4$ $\mu m^3$ (calculated from $V = \pi h_0\left(3a^2 + h_0^2\right)/6$), $\Theta = 22^\circ$ leading to $\lambda = 0.430$, and an evaporation time of $\Delta t = 0.27$ s. The central height $h_0$ and the volume $V$ decreased approximately linearly with time and we have $dh_0/dt \approx -11.0/0.27\ \mu m \cdot s^{-1} = -41\ \mu m \cdot s^{-1}$ and $dV/dt \approx -6 \times 10^4/0.27\ \mu m^3 \cdot s^{-1} = -2.2 \times 10^5\ \mu m^3 \cdot s^{-1}$. For toluene evaporating from PS we used an initial central height of $h_0 = 9.5$ μm, a contact radius of $a = 81$ μm, an initial volume of $V = 10^5\ \mu m^3$, $\Theta = 13^\circ$ leading to $\lambda = 0.461$, and an evaporation time of $\Delta t = 0.33$ s leading to $dh_0/dt = -29\ \mu m \cdot s^{-1}$ and $dV/dt = -3.0 \times 10^5\ \mu m^3 \cdot s^{-1}$.

## Diffusion

After dissolution, the polymer diffuses in the liquid drop. Within $\Delta t$, the characteristic time scale for the evaporation, a typical diffusion length is $\sqrt{6D\Delta t}$, where $D$ is the diffusion coefficient of the polymer in the solvent. For PS in toluene it can be estimated from the phenomenological scaling law $D = D_0 \exp(-\alpha c^u)$,[37] with $D_0 = 2.8 \times 10^{-8}$ $\overline{M}_w^{-0.55}$ $m^2 \cdot s^{-1}$[38] ($\overline{M}_w$ in $g \cdot mol^{-1}$), $u = 0.65$, and $\alpha = 15$.[39] The diffusion coefficient in the dilute regime is $1.2 \times 10^{-10}$ $m^2 \cdot s^{-1}$ for $\overline{M}_w = 20.9$ kDa and $1.1 \times 10^{-11}$ $m^2 \cdot s^{-1}$ for $\overline{M}_w = 1\,445$ kDa. Within 0.33 s, a 20.9 kDa PS chain typically diffuses 15 μm. For a 1 445 kDa PS molecule, the diffusion length is 5 μm. We do not know the diffusion coefficient of PEMA in ethyl acetate, but considering that the viscosities of the solvents are roughly the same (0.43 cP for ethyl acetate and 0.65 cP for toluene) we believe the diffusion constants to be not very much different.

Evaporation processes of solutions can be classified with respect to fast and slow evaporation using the Fourier number $Fo = \tau_{evap}/\tau_{diff}$.[40] Here $\tau_{evap} \approx 0.3$ s is the characteristic evaporation time. The characteristic diffusion time for a solute in the solvent, $\tau_{diff}$, can be estimated from the characteristic size of the drops and the diffusion coefficient. With a characteristic size of 100 μm and a diffusion coefficient between $D_{PS} = 1.2 \times 10^{-10}$ and $1.1 \times 10^{-11}$ $m^2 \cdot s^{-1}$ for PS in toluene ($\overline{M}_w = 20.9$ kDa and 1 445 kDa, respectively) the characteristic diffusion time can be estimated by $\tau_{diff} = (10^{-4}m)^2/D_{PS}$. The Fourier numbers obtained as $Fo = 10^{-2}$ to $10^{-3}$ are much lower than unity. Thus we have a case of fast evaporation.

## Crater- and Dot-Like Structures

For ethyl acetate on PEMA only crater-like structures are observed. Clearly the evaporation-driven flow dominates structure formation. This is not surprising when compar-


© 2007 WILEY-VCH Verlag GmbH & Co. KGaA, Weinheim

ing typical time and length scales. Assuming diffusion coefficients like for PS in toluene of the order of $D = 10^{-11}$–$10^{-10}$ $m^2 \cdot s^{-1}$ the distance a polymer diffuses in 0.27 s is 4–13 μm. At a radius of 30 μm the flow velocity calculated with Equation (7) is 91 $\mu m \cdot s^{-1}$. Thus within 0.27 s, a distance of 25 μm is covered. The evaporation-driven flow will thus dominate the whole process and craters are formed.

For toluene on PS the situation is different because the flow velocities are lower (Figure 7). In addition, more polymer is dissolved, in particular for low and intermediate molar masses. Dissolution is further enhanced for multiple drops because not all the toluene evaporates completely within the time interval between two subsequent drops: part of it diffuses into the polymer and remains there before the next drop is deposited. Dissolved polymer increases the viscosity of the liquid and further decreases the evaporation-driven flow. Thus diffusion is more dominant and dot-like structures can be formed. This explains the dot-like structures formed at low and intermediate molar masses. To explain the detailed features, the extent of the dissolution, the evaporation-driven flow, and the diffusion have to be known locally. This can only be achieved with future quantitative simulations.

In previous experiments with toluene on PS, mainly crater-like structures were observed.[15,36] The reasons are the different length and time scales of these experiments. Drops were deposited by a micropipette. As a result the initial volume ($2 \times 10^6$ $\mu m^3$) and contact radius (≈200 μm) was larger and the apparent evaporation time (5 s) was longer. This reduces the influence of diffusion and the evaporation-driven flow dominates, leading to the formation of crater-like structures.

## Optical Determination of the Molar Mass of PS

The topographies of the surface structures, namely the height/depth of the center and the asymmetry, are characteristic enough to obtain information about the molar mass of the underlying PS substrate. In the series of ten polymers used, each one could be discriminated from the topography and thus its molar mass could be determined. Based on this series, in which each polymer had an average molar mass 1.5 times greater than the previous one, the accuracy is of the order of 50%.

Analyzing the molar mass by depositing a drop of solvent onto the polymer and observing the evaporation structure is an almost non-invasive method, because the height changes are in the sub-10 μm range. This advantage, on the other hand, poses a problem: it requires expensive equipment to quantitatively measure the topography. Therefore, we tried a simple alternative, which does not give the precise topography, but might be sufficient to determine the molar mass after calibration. A camera (objective lens plus imaging plane) was positioned approximately 2.8 cm above the polymer sample and adjusted so that the planar polymer surface (beside the structure) was in focus (Figure 8). The polymer sample was illuminated from below with a parallel light beam. The structure diffracts the light in a characteristic way. A large fraction of the shape of evaporation structures can be described as spherical;[14] they act like a focusing or divergent lens. For example, for PS with an intermediate molar mass, the structure diverges the light

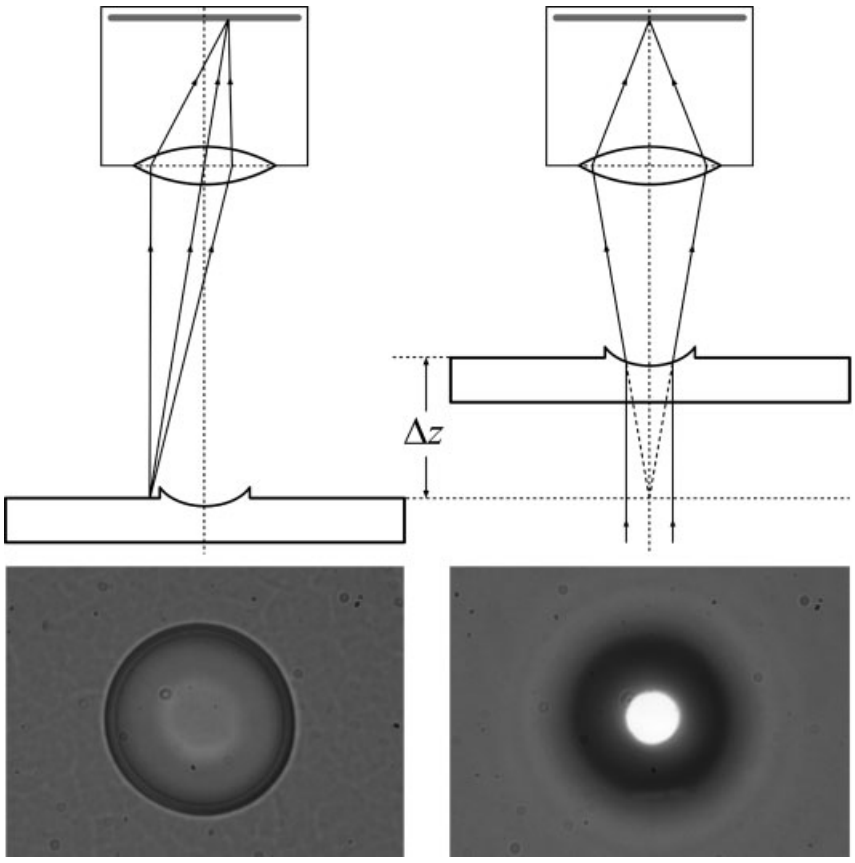


*Figure 8.* Optical set-up for characterizing the shape of evaporation structures. As an example, in the bottom half, pictures are shown that were taken in the respective positions of a PS sample of $\overline{M}_w = 210$ kDa, after evaporation of a toluene drop placed by a syringe.


*Macromol. Chem. Phys.* **2007**, *208*, 2134–2144
© 2007 WILEY-VCH Verlag GmbH & Co. KGaA, Weinheim
DOI: 10.1002/macp.200700122

beam owing to the concave shape. To compensate for this diverging light the camera has to be moved closer to the sample by a distance $\Delta z$. The divergence is just compensated, when this distance is equal to the focal point of the structure.

### Dependence of the Optical Properties on the Molar Mass

To characterize the optical properties of the evaporation structures in detail we used laser scanning confocal microscopy (LSCM) in transmitted- and reflected-light configuration (Figure 9A). LSCM has the ability to collect light from thin optical slices. By moving the focal plane, a stack of slices can be created in order to extract three-dimensional images or cross-sections from different planes. The substrates were placed onto a motorized *xy* stage above the objective with the evaporation structures facing down. They were illuminated from above by a red laser and from below by a green laser. The light intensity was imaged, starting 2.5 mm below the surface. The vertical distance between the measured slices was 35 μm. For each slice the red light, and at the same time, the green light was detected. From each stack a cross-section in the *xz* plane at the center of the evaporation structure was taken as shown in Figure 9B. The position of the upper and lower surfaces of the substrate, determined from the reflected light, is indicated in the figure and can be used as a reference. For a better comparison with the corresponding three-dimensional topologies (lower panel of Figure 9B), a cross-section is displayed with the structure facing up.

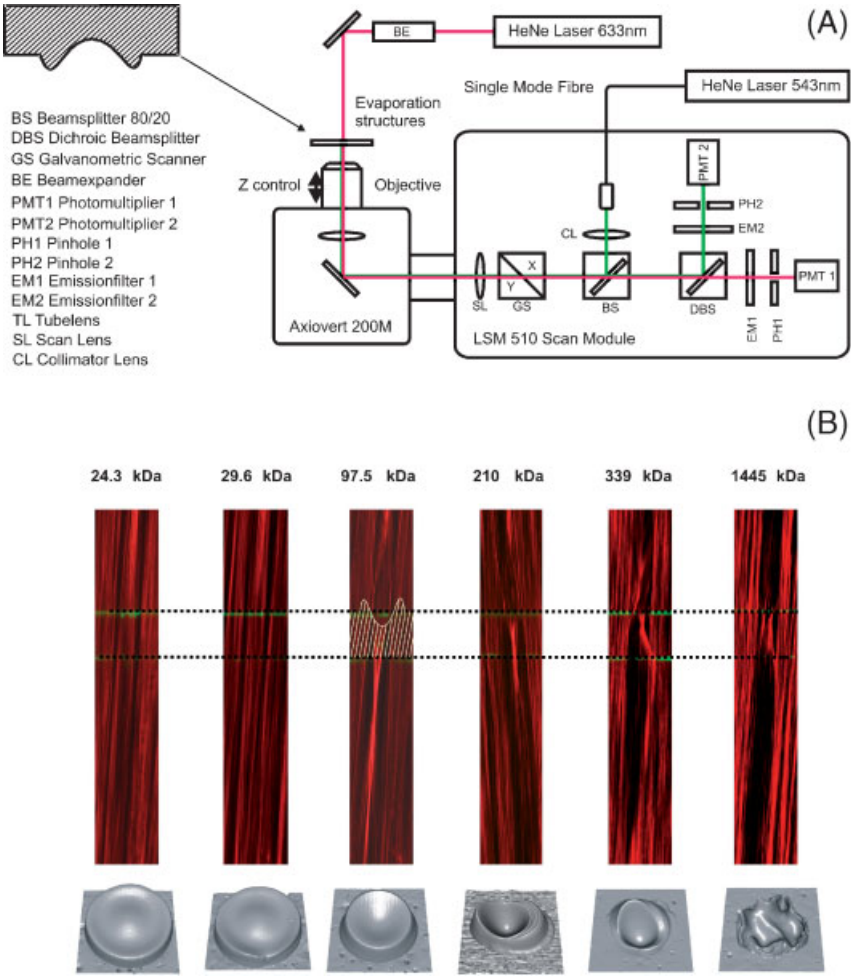


*Figure 9.* (A) Scheme of the modified laser scanning confocal microscopy setup in order to measure the transmitted and reflected light simultaneously. (B) *xz* sections from the center of merged stacks, measured in transmission and reflection. The dotted, horizontal lines indicate the reflected light from the upper and lower surfaces of the substrate, whereas the red light indicates the transmitted light. The images of microstructures prepared on polystyrene with molar masses ranging from 24.3 to 1 445 kDa are compared with the corresponding three-dimensional topologies.

Evaporation structures are related to the polymer molar mass, especially in the toluene/PS system. Alternatively, one might be able to predict the polymer structure by the optical properties of such structures. Since the evaporation structure changes from convex to concave to asymmetric and then into irregular, the distribution of light intensities varies accordingly (Figure 9). For PS with a molar mass below 29.6 kDa, the focus spot was found above the substrate top surface, for molar masses between 97.5 and 210 kDa, a focal spot was observed in the opposite direction, which is below the reverse side of the substrate. The distance between the focal spot and reverse substrate surface became shorter and shorter with increasing polymer molar mass. As the polymer molar mass increased to 339 kDa or 643 kDa, a distorted focus spot appeared inside of the substrate, since the structure was asymmetric. For molar masses above 1 000 kDa more than one peak in the light intensity can be found, due to the multiple peaks and wells formed. For making microlenses, a molar mass of 90 to 210 kDa is most suitable and the focal length could be adjusted by choosing the appropriate molar mass.

## Conclusion

Evaporation structures left by microscopic solvent drops on polymer surfaces


© 2007 WILEY-VCH Verlag GmbH & Co. KGaA, Weinheim

are characteristic of the specific polymer/solvent combination and the molar mass of the polymer. Solvent evaporates at constant contact radius from a polymer surface. The shape of the evaporation structures is determined by at least four processes: the dissolution of the polymer, the evaporation-driven radial flow of the solvent, the diffusion of dissolved polymer molecules, and swelling of the polymer. Depending on which of these processes dominates different topologies can be formed. If, on the time scale of evaporation, the dissolved molecules diffuse a larger distance than covered by evaporation-driven flow, dot-like structures are formed. If evaporation-driven flow dominates, crater-like structures prevail. The amount of dissolved polymer influences this relation by increasing the viscosity and thus reduces evaporation-driven flow. This also explains why dot-like structures are only found for microdrops. In large drops, diffusion is less significant, evaporation-driven flow dominates and crater-like structures are formed. For ethyl acetate/PEMA, only concave structures were observed, which we attribute to a reduced rate of dissolution as compared to PS/toluene.

For toluene evaporating from polystyrene the evaporation structures were characteristic for the molar mass. Change in the molar mass by 50% led to detectable changes in the evaporation structures. Before the method can be used to measure the molar mass of a specific polymer, a better understanding of the evaporation process is required; namely, the role of entanglements in the dissolution rate, the flow pattern of the solvent, the mobility of the polymer at different solvent concentrations, and possible temperature gradients require a better understanding.

Acknowledgements: The authors thank *Thomas Wagner* for providing the polystyrene. This research was supported by the *Deutsche Forschungsgemeinschaft* (GR2003/2) within the research group FOR 516.

Received: March 6, 2007; Revised: May 8, 2007; Accepted: May 9, 2007; DOI: 10.1002/macp.200700122

Keywords: coffee-stain effect; drop evaporation; ink-jet; poly (ethyl methacrylate); polystyrene (PS); polymer surfaces

[1] H. W. Morse, *Proc. Am. Acad. Arts Sci.* **1910**, *45*, 363.
[2] I. Langmuir, *Phys. Rev.* **1918**, *12*, 368.
[3] R. G. Picknett, R. Bexon, *J. Colloid Interface Sci.* **1977**, *61*, 336.
[4] R. N. O'Brien, P. Saville, *Langmuir* **1987**, *3*, 41.
[5] S. M. Rowan, M. I. Newton, G. McHale, *J. Phys. Chem.* **1995**, *99*, 13268.
[6] C. Bourgès-Monnier, M. E. R. Shanahan, *Langmuir* **1995**, *11*, 2820.
[7] A. J. H. McGaughey, C. A. Ward, *J. Appl. Phys.* **2002**, *91*, 6406.
[8] H. Y. Erbil, G. McHale, M. I. Newton, *Langmuir* **2002**, *18*, 2636.
[9] Y. Takata, S. Hidaka, A. Yamashita, H. Yamamoto, *Int. J. Heat Fluid Flow* **2004**, *25*, 320.
[10] H. Hu, R. G. Larson, *Langmuir* **2005**, *21*, 3972.
[11] C. Poulard, G. Guéna, A. M. Cazabat, A. Boudaoud, M. Ben Amar, *Langmuir* **2005**, *21*, 8226.
[12] E. Bonaccurso, H.-J. Butt, *J. Phys. Chem. B* **2005**, *109*, 253.
[13] S. David, K. Sefiane, L. Tadrist, *Colloids Surf. A: Physicochem. Eng. Aspects* **2007**, *298*, 108.
[14] E. Bonaccurso, H.-J. Butt, B. Hankeln, B. Niesenhaus, K. Graf, *Appl. Phys. Lett.* **2005**, *86*, 124101.
[15] G. Li, N. Höhn, K. Graf, *Appl. Phys. Lett.* **2006**, *89*, 241920.
[16] T. Kawase, H. Sirringhaus, R. H. Friend, T. Shimoda, *Adv. Mater.* **2001**, *13*, 1601.
[17] B.-J. de Gans, U. S. Schubert, *Langmuir* **2004**, *20*, 7789.
[18] E. Tekin, B.-J. de Gans, U. S. Schubert, *J. Mater. Chem.* **2004**, *14*, 2627.
[19] E. Bonaccurso, H.-J. Butt, K. Graf, *Eur. Polymer J.* **2004**, *40*, 975.
[20] H. Y. Erbil, Y. Avci, *Langmuir* **2002**, *18*, 5113.
[21] C. Stupperich-Sequeira, K. Graf, W. Wiechert, *Mathematical Comput. Modelling Dynamical Syst.* **2006**, *12*, 263.
[22] J. Conway, H. Korns, M. R. Fisch, *Langmuir* **1997**, *13*, 426.
[23] R. D. Deegan, O. Bakajin, T. F. Dupont, G. Huber, S. R. Nagel, T. A. Witten, *Nature* **1997**, *389*, 827.
[24] R. D. Deegan, O. Bakajin, T. F. Dupont, G. Huber, S. R. Nagel, T. A. Witten, *Phys. Rev. E* **2000**, *62*, 756.
[25] H. Hu, R. G. Larson, *J. Phys. Chem. B* **2002**, *106*, 1334.
[26] B. Rieger, L. R. van den Doel, L. J. van Vliet, *Phys. Rev. E: Stat. Nonlinear Soft Matter Phys.* **2003**, *68*, 036312.
[27] A. J. Petsi, V. N. Burganos, *Phys. Rev. E: Stat. Nonlinear Soft Matter Phys.* **2006**, *73*, 041201.
[28] T. Kajiya, E. Nishitani, T. Yamaue, M. Doi, *Phys. Rev. E: Stat. Nonlinear Soft Matter Phys.* **2006**, *73*, 011601.
[29] Y. Gorand, L. Pauchard, G. Calligari, J. P. Hulin, C. Allain, *Langmuir* **2004**, *20*, 5138.
[30] E. Bormashenko, R. Pogreb, A. Musin, O. Stanevsky, Y. Bormashenko, G. Whyman, O. Gendelman, Z. Barkay, *J. Colloid Interface Sci.* **2006**, *297*, 534.
[31] S. T. Chang, O. D. Velev, *Langmuir* **2006**, *22*, 1459.
[32] M. Gonuguntla, A. Sharma, *Langmuir* **2004**, *20*, 3456.
[33] L. J. Fetters, D. J. Lohse, S. T. Milner, W. W. Graessley, *Macromolecules* **1999**, *32*, 6847.
[34] *Polymer Handbook*, 4th edition, J. Brandrup, E. H. Immergut, E. A. Grulke, Eds., John Wiley & Sons, New York 1999.
[35] S. Wu, *J. Polymer Sci., Part B: Polym. Phys.* **1989**, *27*, 723.
[36] G. Li, H.-J. Butt, K. Graf, *Langmuir* **2006**, *22*, 11395.
[37] G. D. J. Phillies, *Macromolecules* **1986**, *19*, 2367.
[38] G. Min, D. Savin, Z. Gu, G. D. Patterson, S. H. Kim, D. J. Ramsay, D. Fishman, I. Ivanov, E. Sheina, E. Slaby, J. Oliver, *Int. J. Polym. Analysis Characterization* **2003**, *8*, 187.
[39] R. Liu, X. Gao, J. Adams, W. Oppermann, *Macromolecules* **2005**, *38*, 8845.
[40] E. Bormashenko, Y. Bormashenko, R. Pogreb, O. Stanevsky, G. Whyman, T. Stein, M. H. Itzhaq, Z. Barkay, *Colloids Surf. A: Physicochemical Eng. Aspects* **2006**, *290*, 273.


© 2007 WILEY-VCH Verlag GmbH & Co. KGaA, Weinheim